

SM Journal Clinical and Medical Imaging

Research Article

Microwave-Assisted Synthesis of Small and Water-Dispersible Lanthanide-Doped NaGdF₄ Nanocrystals for PL/CT/ MR Multimodal Imaging

SongxiaYu¹, Zhiqiang Wang², Ruijun Cao¹ and Lingjie Meng¹*

¹Department of Chemistry, School of Science, Xi'an Jiaotong University, PR China ²Science Research, Northwest Institute of Nuclear Technology, PR China

Article Information

Received date: Dec 01, 2016 Accepted date: May 05, 2017 Published date: May 12, 2017

*Corresponding author

Lingjie Meng, Department of Applied Chemistry, School of Science State Key Laboratory for Mechanical Behavior of Materials, Xi'an Jiaotong University, Xi'an, 710049, PR China, Email: menglingjie@mail.xjtu.edu.cn

Distributed under Creative Commons CC-BY 4.0

Keywords NaGdF₄; Photoluminescence (PL); X-ray computed tomography (CT); Magnetic resonance (MR); Imaging microwave-assisted solvothermal reaction

Abstract

Multimodal imaging is advantageous in overcoming the deficiencies of individual imaging modalities. Herein, small, monodisperse and water-dispersible NaGdF $_4$: Ln (Ln = Eu, Tb, Dy) Nano Crystals (NCs) were successfully prepared in a facile manner by one-pot microwave-assisted solvothermal reaction in ethylene glycol. The morphology, size distribution, zeta potential, and crystal structure of the resulting NCs were well characterised by transmission electron microscopy, Nano-ZS90 Zetasizer, and X-ray diffraction analyses. These as-synthesised NaGdF $_4$: Ln (Ln = Eu, Tb, Dy) NCs exhibited a low cytotoxicity for Hela and C9H2 cells. Moreover, the doping concentrations of Eu $^{3+}$, Tb $^{3+}$, and Dy $^{3+}$ ions were optimised for efficient Photoluminescence (PL) under the excitation of 273 nm in water. Furthermore, these NCs exhibited excellent relaxivity parameters (r,) in Magnetic Resonance (MR) imaging and Hounsfield units in X-ray Computed Tomography (CT) imaging *in vitro*. Therefore, these NCs have great potential to construct a unique platform for PL/CT/MR multimodal imaging simultaneously.

Introduction

Frequently used imaging techniques in clinical practice include ultrasound, Photoluminescence (PL), Magnetic resonance (MR), and X-ray Computed Tomography (CT) [1-4]. However, each modality imaging technique is often restricted by its nature. For example, PL imaging has excellent sensitivity, but is often restricted by the depth of penetration in tissues and organs, and it is difficult to obtain accurate anatomical and physiological information. In contrast, ultrasound, CT, and MR imaging techniques have a low sensitivity, but their high spatial resolution can provide exceptional three-dimensional (3D) anatomical information of organs and tissues [5,6]. Therefore, multimodal imaging by combining two or more complementary imaging modalities into one system has attracted much attention, offering a synergistic improvement of diagnostic ability over a single imaging modality.

Several multimodal imaging probes have been developed to facilitate the real-time assessment of pathways and mechanisms *in vivo* for improved diagnostic efficacy [7,8]. These complementary multimodal imaging techniques provide a high spatial resolution and high sensitivity. However, multifunctional materials suffer from large sizes, complex structures, and time-consuming multistep preparation methods. Therefore, it is necessary to design and develop various optimal nanostructures to balance low cost, high performance, and multiple functions.

In the recent years, lanthanide (Ln³+)-doped PL nanocrystals (NCs) have attracted much interest owing to their fascinating optical properties including large Stokes shifts, sharp emission bands, long fluorescence lifetimes, and high resistance to photobleaching and photochemical degradation [9-11]. The Ln3+-doped PL materials have been investigated for diverse applications in various fields such as displays, lighting, lasers, optical amplifiers, biological labels, and biological imaging [12-16]. The choice of a suitable host matrix is of great significance in designing efficient Ln3+-doped PL materials. Among various rare-earth compounds, fluorides are ideal host candidates owing to close lattice matches to dopant ions for a high Ln3+ solubility, low phonon frequencies, high quantum efficiency, and good thermal stability [17,18]. Among these, NaGdF, NCs are considered as an excellent PL host matrix for various optically active Ln³+ [19,20]. Moreover, Gd³+ has seven unpaired electrons that can efficiently alter the spin-spin relaxation time of surrounding water protons [14,21,22]. Therefore, Gd3+-containing materials have been developed as potential T,-weighted MR imaging contrast agents for biomedical applications [23,24]. Generally, T, contrast agent with a bright signal is more desirable than T₂ contrast agent with a dark signal, because the intrinsic dark signal in T2-weighted MR imaging can mislead the clinical diagnosis [25,26]. Furthermore, Ln3+ elements have intrinsic advantages for CT imaging owing to a higher X-ray absorption efficiency. To sum up, this special characteristic of Ln3+-doped NaGdF4 NCs makes them suitable for efficient PL/CT/ /MR multimodal imaging.



SMGr\$up

Copyright © Meng L

Various methods have been used to prepare Ln³+-doped NaGdF₄ NCs, including hydrothermal method, thermal decomposition, chemical precipitation, solvothermal synthesis, and microwave-assisted hydrothermal synthesis [18,27-30]. So far, the thermal decomposition method has been regarded as the most successful method to prepare monodisperse Ln³+-doped NaGdF₄ NCs with uniform morphology and small size [4,31]. However, this method has some drawbacks such as rigorous experimental conditions and hazardous precursors. Particularly, complex surface modification processes are necessary to convert the as-synthesised hydrophobic NCs into hydrophilic NCs. One-pot hydrothermal methods have also been widely used to synthesize Ln³+-doped NaGdF₄ NCs [32-35]. Although hydrothermal methods are efficient for controlling the morphology of products and improving their purity and crystallization, they are usually time-consuming and afford hexagonal rods with low yields.

Herein, a simple but effective method is reported for synthesizing small and water-dispersible NaGdF₄:Ln (Ln = Eu, Tb, Dy) NCs by a one-pot microwave-assisted solvothermal route in Ethylene Glycol (EG) with EDTA-2Na as the morphology-controlling agent. The polar EG not only serves as the reaction solvent, but also acts as the surface-capping agent to prevent the growth of nanoparticles. The dopant concentrations were optimised for efficient PL by adjusting the doping concentrations of Eu³⁺, Tb³⁺, and Dy³⁺ ions. The *in vitro* cytotoxicity of resulting nanoparticles was assessed by the typical WST-1 assays using HeLa and C9H2 cells separately. Furthermore, the MR and CT contrast capacities of the as-synthesised NCs with different doping concentrations of Eu³⁺, Tb³⁺ and Dy³⁺ ions were also investigated.

Experimental Section

Chemicals

Gd (NO $_3$) $_3$ ·6H $_2$ O (99.9%), EuCl $_3$ ·6H $_2$ O (99.9%), Tb (NO $_3$) $_3$ ·6H2O (99.9%), and Dy(NO $_3$) $_3$ ·5H $_2$ O (99.9%) were purchased from Sigma-Aldrich. Ammonium fluoride (NH $_4$ F, A.R.) and sodium hydroxide (NaOH, A.R.) were purchased from Aladdin Reagents. Ethylenediaminetetraacetic acid disodium salt (EDTA-2Na, 99.0%) was obtained from Tianjin Zhiyuan Chemical Reagent. EG (A.R.) was purchased from Haotian Chemical Reagent. All the chemicals were used as received without further purification.

Synthesis of NaGdF₄:Ln (Ln = Eu, Tb, Dy) NCs

 $NaGdF_{a}:x\%Eu (x = 13,16,19,22), NaGdF_{a}:x\%Tb (x = 10,13,16,19),$ and NaGdF₄:x%Dy (x = 1,4,7,10) NCs were prepared by a similar one-pot microwave-assisted solvothermal reaction with EG as the solvent. In a typical synthesis of NaGdF₄:x%Eu (x = 13,16,19,22), 0.5 mmol (total amount) of rare-earth precursors (0.435 mmolGd (NO₃)₃·6H₂O + 0.065 mmol EuCl₃·6H₂O, 0.42 mmolGd (NO₃)₃·6H₂O + 0.08 mmol EuCl₃·6H₂O, 0.405 mmolGd (NO₃)₃·6H₂O + 0.095 mmol $EuCl_3 \cdot 6H_2O$, 0.39 mmolGd (NO₃)₃ · 6H₂O + 0.11 mmol $EuCl_3 \cdot 6H_2O$) was respectively dissolved in EG (28 mL), followed by the addition of 0.093 g EDTA-2Na. The obtained solution was magnetically stirred at room temperature until a homogeneous solution was obtained. Then, NaOH (0.05 g) and NH₄F (0.074 g) were dissolved in EG (4 mL), and the solution was injected into the reaction mixture under stirring. The mixture was introduced into a microwave reaction kettle and heated at 240 °C for 1 h with a power of 800 W in a microwave hydrothermal reactor (XH-800S, Xianghu Technology). The mixture

was cooled to room temperature naturally. The product was isolated by centrifugation at 10,000 rpm for 10 min, washed sequentially with deionised water and ethanol, and re-dispersed in deionised water (5 mL) to form a transparent colloidal solution.

Instruments and characterization

The TEM images were obtained using a JEOL JEM-2100HR TEM operating at 200 kV. The XRD patterns were collected using a Bruker D2 PHASER X-ray diffractometer using CuK α radiation (λ = 1.5418 Å) with an operating voltage of 30 kV and a current of 10 mA. The diffraction patterns were collected from 15° to 70° at a speed of 3°·min⁻¹. The DLS and zeta potential measurements were performed using a Nano-ZS90 Zetasizer (Malvern, UK) at 25°C. The Cell viability was assessed by in vitro WST-1 assays in Hela and C9H₂ cells separately. The PL spectra were recorded at room temperature using an Edinburgh steady-state fluorescence spectrometer FLS920 with an excitation wavelength of 273 nm. The PL digital photographs were recorded using a Canon D70 camera. The CT imaging was obtained at 120 kVp voltages using a Philips 260-slice CT scanner (Philips Medical System). The relaxivity parameters and T₁-weighted MR images were recorded using a 0.52 T MR scanner with MiNiMR60-Analyst (Shanghai Niumag, China).

Cytotoxicity assay in vitro

The cell cytotoxicity of NCs was measured by WST-1 assay. In brief, HeLa and H9C2 cells were seeded in 96-well plates at a density of $5\times10_4$ per well for 24 h. The cells were treated with a specific concentration of NaGdF4:16% Eu, NaGdF4:13% Tb, and NaGdF4:4% Dy NCs (10 μg mL $^{-1}$, 25 μg mL $^{-1}$, 50 μg mL $^{-1}$, and 100 μg mL $^{-1}$) at 37 °C for 24 h. Then, the cell viability was determined by adding 10 μL WST-1 reagent. The optical densities were read at 450 nm using a microplate spectrophotometer (Spectra Max 190; Molecular Devices). The cells cultured without NCs over the same time were used as the controls. The cell viability was calculated as the percentage of absorbance of the sample well compared to that of the control well containing untreated cells.

CT imaging in vitro

To assess the CT contrast efficacy, the *in vitro* CT imaging was carried using a Philips 256-slice CT scanner operated at 120 kVp voltages. A series of aqueous solutions of NaGdF $_4$:16% Eu, NaGdF $_4$:13% Tb, and NaGdF $_4$:4% Dy NCs at different concentrations (0 mg/ mL, 1.25 mg/mL, 2.5 mg/mL, 5 mg/mL, 10 mg/mL, and 20 mg/ mL) in 2 mL Eppendorf tubes were prepared. The 3D datasets were reconstructed with a voxel size of 20 μm . The CT imaging parameters are as follows: A slice thickness of 0.9 mm, a pitch of 0.99, 120 kVp, 300 mA, a field of view with 350 mm, a gantry rotation time of 0.5 s, a table speed of 158.9 mms $^{-1}$. The axial images were reformed to coronal images using a computational technique known as multiplanar reconstruction.

T₄-weighted MR imaging in vitro

The longitudinal relaxation time T_1 and corresponding T_1 -weighted MR images of NaGdF₄:16% Eu, NaGdF₄:13% Tb, and NaGdF₄:4% Dy NCs at different Gd³⁺ concentrations (0 mmol L⁻¹, 0.125 mmol L⁻¹, 0.25 mmol L⁻¹, 1 mmol L⁻¹, and 2 mmol L⁻¹) were acquired using a MR imaging instrument with 0.52 T magnetic field

SMGr\$up Copyright @ Meng L

with MiNiMR60-Analyst (Shanghai Niumag, China). The obtained NCs in water as the contrast agent were placed in a series of 2 mL centrifuge tubes for T1 measurement. The resulting T₁ values were recorded at different Gd3+ concentrations and plotted as 1/T, (R1) for NaGdF₄:16% Eu, NaGdF₄:13%Tb, and NaGdF₄:4%Dy NCs; the slopes of these lines provided the r₁ values. The T₁-weighted MR images were collected using the parameter setting as follows: Echo Time (TE) = 30 ms, Repetition Time (TR) = 4500 ms, SW = 100 Hz, NS = 4, slices = 1, slice thickness = 1 mm.

Results and Discussion

Morphology and size distributions of NaGdF,:Ln (Ln = Eu, Tb, Dy) NCs

The morphology and sizes of the as-synthesised NaGdF,:Ln (Ln = Eu, Tb, Dy) NCs were investigated by transmission electron microscopy (TEM) (Figure 1). NaGdF,:16% Eu, NaGdF,:13% Tb, and NaGdF₄:4% Dy NCs have uniform and almost monodisperse spherical morphology, and their average sizes measured using image J software from ~100 collected data were approximately 36 nm, 37 nm, and 35 nm, respectively. Because the ionic radius of Eu³⁺, Tb³⁺, and Dy3+ is similar to that of Gd3+, the doped Eu3+, Tb3+, and Dy3+ did not change the morphology and sizes of the as-synthesised NCs. For the same reason, the dopant concentrations of various Eu³⁺, Tb³⁺, and $\mathrm{D}\mathrm{y}^{\scriptscriptstyle{3+}}$ ions have a negligible effect on the morphology and size of the as-obtained NaGdF, NCs. The morphology and size of the as-synthesised NaGdF₄:Ln (Ln = Eu, Tb, Dy) NCs were investigated (Figures S1-S3). NaGdF4 NCs tend to grow into several hundred nanorods in an aqueous solution. Here, polar EG was used as both the reaction solvent and surface-capping agent, preventing the growth of nanoparticles. Dynamic Light Scattering (DLS) analyses were also carried out to characterize the corresponding aqueous dispersion of the resultant NCs (Figure S4). The relatively narrow particle size distributions in water with average hydrodynamic diameters of approximately 100 nm were consistent with the TEM

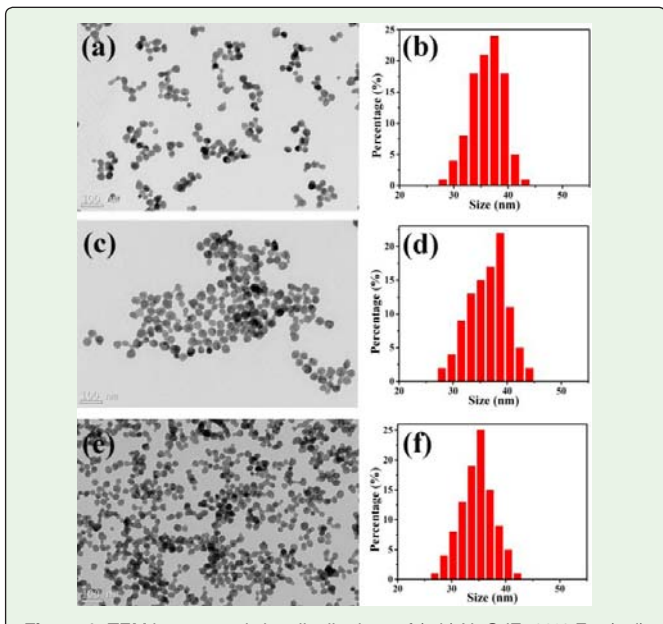


Figure 1: TEM images and size distributions of (a,b) NaGdF₄:16% Eu, (c,d) NaGdF₄:13% Tb, and (e,f) NaGdF₄:4% Dy.

NaGdF4:4%Dy Intensity (a.u.) NaGdF4:13%Tb NaGdF4:16%Eu JCPDS No.27-0699 50 40 60 2θ (degree) Figure 2: XRD patterns of NaGdF,:16% Eu, NaGdF,:13% Tb, and

NaGdF₄:4% Dy NCs.

results. Commonly, it is vital to control the size of nanomedicines (generally <120 nm) for cellular delivery. Therefore, these synthesised NCs are small enough for bioimaging. EDTA-2Na was used as the morphology-controlling agent and played a vital role in the morphology of NCs. EDTA moieties might have attached to the surface of NCs to help the growth of monodisperse nanoparticles. Otherwise, NaGdF₄:16% Eu NCs without the protection of EDTA-2Na showed irregular and adhesive morphology (Figure S5).

XRD characterization

The crystal structures of the obtained NaGdF₄:16%Eu, NaGdF_a:13%Tb, and NaGdF_a:4%Dy NCs were studied by X-ray diffraction (XRD) analysis (Figure 2). All the three samples showed good crystallinity and similar diffraction peaks. All the identified diffraction peaks for these samples matched with the standard hexagonal phase of β-NaGdF₄ (JCPDS card no. 27–0699). The doped Eu³⁺, Tb³⁺, and Dy³⁺ did not change the crystalline phase, probably because their ionic radius is approximately equal to that of Gd³⁺. Moreover, no trace impurity peak was observed in the XRD patterns, indicating that all the samples are in a single phase in the detectable

Zeta potential characterization

Table 1 shows the corresponding zeta potentials of the asobtained NCs. The zeta potentials of NaGdF₄:16% Eu, NaGdF₄:13% Tb, and NaGdF₄:4% Dy NCs in water were approximately 42.5 mV, 34.2 mV, and 38.5 mV, respectively, even though their surfaces were shielded by EG. Their highly positive charge is beneficial to form stable NC dispersions. These NCs were well dispersed in water, forming a transparent solution (Figure S6).

Table 1: Zeta potentials of NaGdF₄: 16% Eu, NaGdF₄:13% Tb, and NaGdF₄: 4% Dy NCs in aqueous solutions.

NCs	Zeta potential(mV)*
NaGdF₄:16%Eu	42.5 ± 0.8
NaGdF ₄ :13%Tb	34.2 ± 1.9
NaGdF ₄ : 4%Dy	38.5 ± 3.6

^{*}All the values were averaged from three measurements.

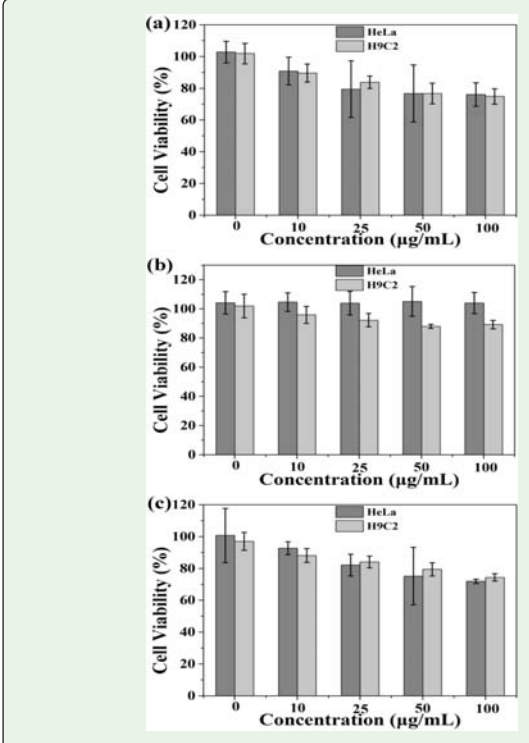


Figure 3: Cell viability of HeLa and H9C2 cells after the culture with (a) $NaGdF_4$: 16% Eu, (b) $NaGdF_4$: 13% Tb, and (c) $NaGdF_4$: 4% Dy NCs at a series of concentrations for 24 h.

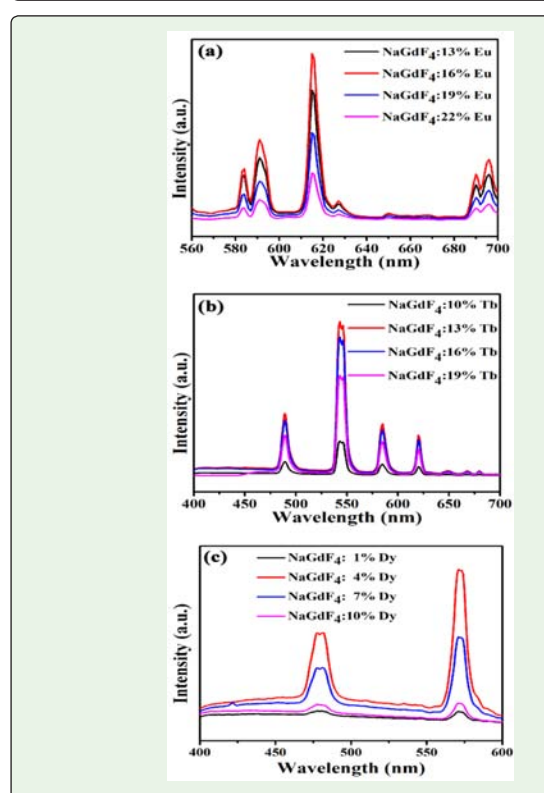


Figure 4: Room-temperature emission spectra of (a) NaGdF₄: x% Eu (x = 13,16,19,22), (b) NaGdF₄: x% Tb (x = 10,13,16,19), and (c) NaGdF₄: x% Dy (x = 1,4,7,10) NCs under the excitation of 273 nm.

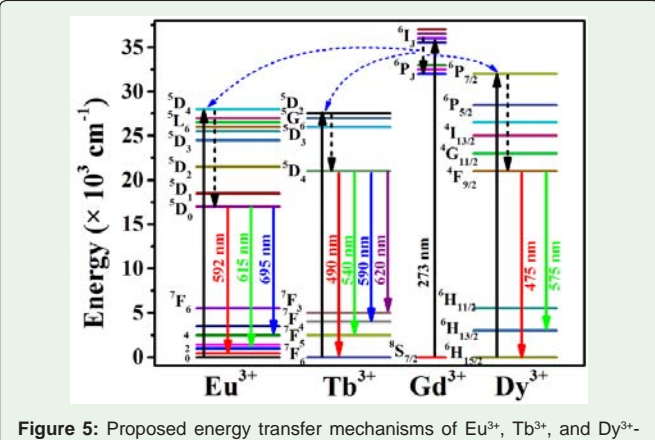


Figure 5: Proposed energy transfer mechanisms of Eu³⁺, Tb³⁺, and Dy³⁺doped NaGdF, NCs.

Cytotoxicity assay in vitro

Biocompatibility is the main issue for any biomaterial. Therefore, the cell cytotoxicityof NaGdF,:16% Eu, NaGdF,:13% Tb, and NaGdF₄:4%Dy NCs were quantitatively measured by WST-1 assays (Figure 3). The HeLa and H9C2 cells were selected as the tumour and normal cell models, respectively. These two types of cells were incubated in DMEM supplemented with 10% FBS containing NaGdF₄:16%Eu, NaGdF₄:13%Tb, and NaGdF₄:4% Dy NCs at different concentrations for 24 h. With the increase in NC concentrations, the cell viability of HeLa and H9C, cells was slightly reduced. However, the cell viability was higher than 71% under all the experimental conditions. Therefore, the as-obtained NaGdF.:16%Eu, NaGdF₄:13%Tb, and NaGdF₄:4%Dy NCs have biologically low cytotoxicity in WST-1 analysis in a wide concentration range from 0 to 100 μg mL⁻¹ and exhibit potential for biomedical applications.

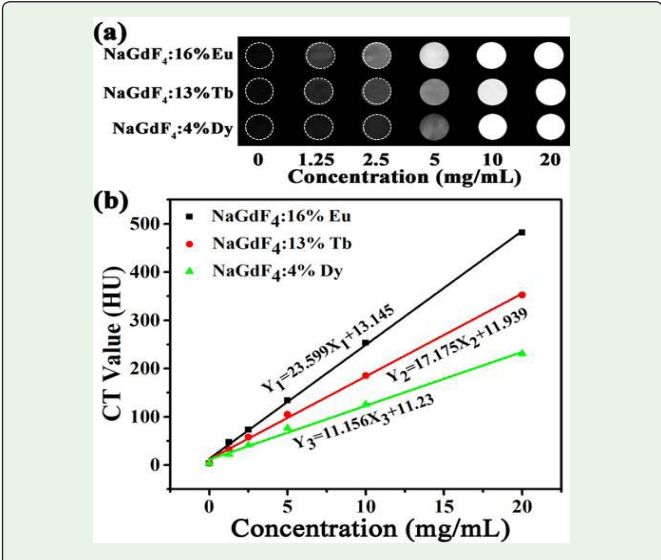


Figure 6: (a) In vitro CT images of NaGdF₄:16% Eu, NaGdF₄:13% Tb, and $NaGdF_4$:4% Dy NCs at different concentrations (0,1.25,2.5,5,10,20 mg/mL). Deionised water (0 mg/mL) was used as the reference. (b) Relaxation rate HU vs. various NP concentrations at room temperature.

PL characterization

To optimize the dopant concentrations of Eu³⁺, Tb³⁺, and Dy³⁺ ions for efficient PL, the fluorescence spectra of crystals were measured at different doping concentrations under the excitation of 273 nm in water (Figure 4). The optimal concentrations of Eu³⁺, Tb³⁺, and Dy³⁺ for efficient PL under 254 nm excitation were 16%, 13%, and 4%, respectively. Below the optimal Ln³⁺-doped concentration, the relatively low PL intensity can be attributed to the low concentration of PL active sites. When the Ln³⁺-doped concentration was above the optimal concentration, the PL intensity decreased gradually. In fact, the PL quenching with increasing doped Ln³⁺ ion concentration is a typical property of Ln³⁺-doped systems, where the distance between the neighbouring doped Ln³⁺ ions decreases with the increase in the dopant Ln³⁺ ion concentration. This decrease in the distance between the doped Ln³⁺ ions results in the cross-relaxation among them, thereby increasing the probability of reduced radiative transition [17].

The PL colours of NaGdF₄:Eu, NaGdF₄:Tb, and NaGdF₄:Dy NCs were red, green, and blue-green under the excitation of 273 nm in water, respectively. Based on energy-matching conditions, the possible energy transfer mechanisms of these NCs are shown in Figure 5. Three emission bands were clearly observed at 580-595 nm, ~615 nm, and 685–700 nm for NaGdF₄: x% Eu (x = 13,16,19,22) NCs (Figure 4a), corresponding to the transitions from the 5_{D0} state to the $7_{\rm Fj}$ (j = 1,2,4) states of Eu³+ ion. Among them, the emission band at ~615 nm was the strongest [36,37]. NaGdF₄:x% Tb (x = 10,13,16,19) NCs had four emission peaks centred at ~490, ~540, ~590, and ~620 nm, respectively, as shown in Figure 4b; they can be attributed to the characteristic transitions from the $5_{\rm D4}$ state to the $7_{\rm Fj}$ (J = 6,5,4,3) states of Tb³+ ion, respectively [15]. Figure 4c shows the corresponding PL spectra of NaGdF₄:x% Dy (x = 1,4,7,10) NCs. The emission peak at ~475 nm can be attributed to the transition from $4_{\rm E9/2}$ state to $6_{\rm H15/2}$

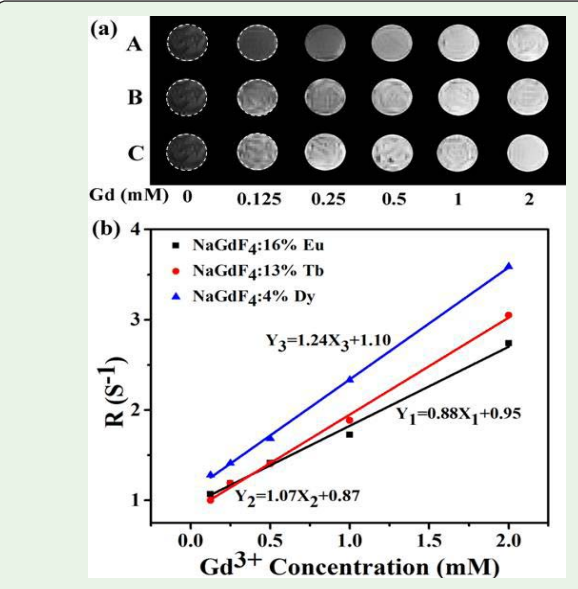


Figure 7: (a) T_1 -weighted MR images of NaGdF₄:16% Eu (A), NaGdF₄:13% Tb (B), and NaGdF₄:4% Dy (C) at various Gd concentrations (0.125,0.25,0.5,1,2 mM). Deionised water (0 mM) was used as the reference. (b) Relaxation rate R1 (1/ T_1) vs. various Gd concentrations of NaGdF₄:16% Eu, NaGdF₄:13% Tb, and NaGdF₄:4%Dy.

 $\label{eq:citation: Yu S, Wang Z, Cao R and Meng L. Microwave-Assisted Synthesis of Small and Water-Dispersible Lanthanide-Doped NaGdF_4 Nanocrystals for PL/CT/MR Multimodal Imaging. SM J Clin. Med. Imaging. 2017; 3(1): 1011.$

state, and the relatively most intense emission band at \sim 575 nm may have originated from the $4_{_{\rm F9/2}}$ \rightarrow $6_{_{\rm H13/2}}$ transition of Dy³+ ion [32].

CT imaging experiments in vitro

CT imaging is frequently used as a clinical diagnosis tool, and Ln3+ elements have intrinsic advantages for CT imaging owing to the higher X-ray absorption efficiency [23]. To assess the CT contrast efficacy of the obtained NaGdF₄:16% Eu, NaGdF₄:13% Tb, and NaGdF₄:4% Dy NCs, in vitro CT imaging was investigated (Figure 6). The signals increased with increasing concentration of NCs, and $NaGdF_{\mbox{\tiny A}}{:}16\%$ Eu NCs had relatively obvious changes in light and shade (Figure 6a). Subsequently, different concentrations of NCs were monitored by X-ray CT to determine the value of Hounsfield unit (HU). A good linear correlation between the HU value and the concentration of NCs was observed (Figure 6b). The slope of each line indicates the contrast effect of each sample. The slopes of NaGdF,:16% Eu, NaGdF₄:13% Tb, and NaGdF₄:4% Dy were 23.599, 17.175, and 11.156, respectively, consistent with those shown in Figure 6a. At equivalent concentrations, the slopes were higher than that of clinical contrast agent iopromide (7.446) [4]. These results show that the asprepared NCs are superior to iopromide as CT imaging agents.

MR Imaging experiments in vitro

The contrast capacities of the obtained NaGdF₄:16%Eu, NaGdF₄:13%Tb, and NaGdF₄:4%Dy NCs were studied at different Gd³⁺ concentrations (0.125-2.0 mM), using deionised water as the control (Figure 7). The signals gradually turned brighter with increasing Gd³⁺ concentration from 0 to 2 mM (Figure 7a), indicating that the NCs acted as T₁-weighted MR imaging contrast agents. From the linear regression fits of the slope of Gd³⁺ concentration-dependent relaxation rate 1/T₁, the relaxivity parameters (r₁) values for NaGdF₄:16% Eu, NaGdF₄:13% Tb, and NaGdF₄:4% Dy NCs were calculated to be 0.88 mM⁻¹S⁻¹, 1.07 mM⁻¹S⁻¹, and 1.24 mM⁻¹S⁻¹, respectively (Figure 7b). These results are consistent with the T₁-weighted MR image measurements. These NCs with relatively good MR contrast capacities have great potentials as MR contrast agents [21,38].

Conclusion

In summary, monodisperse and water-dispersible NaGdF $_4$:Ln (Ln = Eu, Tb, Dy) NCs with 30-40 nm sizes were successfully prepared in a facile manner by one-pot microwave-assisted solvothermal reactions in EG with EDTA-2Na as the capping ligand. These NCs exhibited a low cytotoxicity for Hela and C_9H_2 cells. The doping concentrations of Eu $^{3+}$, Tb $^{3+}$, and Dy $^{3+}$ ions were optimised for efficient PL, achieving strong PL emissions of NaGdF $_4$:16% Eu, NaGdF $_4$:13% Tb, and NaGdF $_4$:4% Dy under the excitation of 273 nm in water. Moreover, the *in vitro* MR and CT imaging studies confirm that the as-obtained NCs exhibited excellent contrast capacities for MR and CT imaging. Therefore, these small, monodisperse, water dispersible, and less toxic NaGdF $_4$:Ln (Ln = Eu, Tb, Dy) NCs have simultaneous PL/CT/MR imaging properties. Thus, they have a great potential for multimodal diagnosis in biological applications.

References

 Tian C, Zhu L, Lin F, Boyes SG. Poly (acrylic acid) Bridged Gadolinium Metal-Organic Framework-Gold Nanoparticle Composites as Contrast Agents for Computed Tomography and Magnetic Resonance Bimodal Imaging. ACS Appl Mater Interf. 2015; 7: 17765-17775. SMGr\$up

Copyright © Meng L

 Sun L, Liu T, Li H, Yang L, Meng L, Lu Q, et al. Fluorescent and Cross-linked Organic-Inorganic Hybrid Nanoshells for Monitoring Drug Delivery. ACS Appl Mater Interf. 2015; 7: 4990-4997.

- Hu Y, Meng L, Niu L, Lu Q. Highly Cross-Linked and Biocompatible Polyphosphazene-Coated Super paramagnetic Fe Langmuir. 2013; 29: 9156-9163.
- Ma D, Meng L, Chen Y, Hu M, Chen Y, Huang C, et al. NaGdF₄:Yb³⁺/ Er³⁺@NaGdF₄:Nd³⁺@Sodium-Gluconate: Multifunctional and Biocompatible Ultrasmall Core—Shell Nanohybrids for UCL/MR/CT Multimodal Imaging. ACS Appl Mater Interf. 2015; 7: 16257-16265.
- Louie A. Multimodality Imaging Probes: Design and Challenges. Chem Rev. 2010; 110: 3146-3195.
- Wu Y, Yang D, Kang X, Li C, Lin J. Facile fabrication of water-soluble Ln³+-doped β-NaGdF₄ nanocrystals (Ln = Ce, Tb, Eu, Dy) with multicolor luminescence and magnetic properties. Mater Res Bull. 2013; 48: 2843-2849.
- Liu B, Li C, Ma P, Chen Y, Zhang Y, Hou Z, et al. Multifunctional NaYF4: Yb, Er@mSiO2@Fe3O4-PEG nanoparticles for UCL/MR bioimaging and magnetically targeted drug delivery Nanoscale. 2015; 7: 1839-1848.
- Chen Q, Wang H, Liu H, Wen S, Peng C, Shen M, et al. Multifunctional Dendrimer-Entrapped Gold Nanoparticles Modified with RGD Peptide for Targeted Computed Tomography/Magnetic Resonance Dual-Modal Imaging of Tumors. Anal Chem. 2015; 87: 3949-3956.
- Wang F, Deng R, Liu X. Preparation of core-shell NaGdF4 nanoparticles doped with luminescent lanthanide ions to be used as up conversion-based probes. Nat Protoc. 2014; 9: 1634-1644.
- Wang R, Li X, Zhou L, Zhang F. Epitaxial Seeded Growth of Rare-Earth Nanocrystals with Efficient 800 nm Near-Infrared to 1525 nm Short-Wavelength Infrared Downconversion Photoluminescence for In Vivo Bioimaging. Angew Chem Int Ed. 2014; 53: 12086-12090.
- Zhou L, Li Z, Ju E, Liu Z, Ren J, Qu X. Aptamer-Directed Synthesis of Multifunctional Lanthanide-Doped Porous Nanoprobes for Targeted Imaging and Drug Delivery. Small9. 2013: 4262-4268.
- Ren G, Zeng S, Hao J. Tunable Multicolor Up conversion Emissions and Paramagnetic Property of Mono dispersed Bifunctional Lanthanide-Doped NaGdF4 Nanorods. J Phys Chem. 2011; 115: 20141-20147.
- Huang X Dual-model upconversion luminescence from NaGdF4:Nd/Yb/Tm@ NaGdF4:Eu/Tb core-shell nanoparticles. J Alloy Compd. 2015; 628: 240-244.
- Xu J, Gai S, Ma P, Dai Y, Yang G, He F, et al. Gadolinium fluoride mesoporous microspheres: controllable synthesis, materials and biological properties. J Mater Chem. B. 2014; 1791-1801.
- Ding M, Chen D, Wan Z, Zhou Y, Zhong J, Xi J, et al. Achieving efficient Tb³⁺ dual-mode luminescence via Gd-sublattice-mediated energy migration in a NaGdF₄ core-shell nanoarchitecture. J Mater Chem. C3: 2015; 5372-5376.
- Wu Y, Li C, Yang D, Lin J. Rare earth β-NaGdF₄ fluorides with multiform morphologies: Hydrothermal synthesis and luminescent properties. J Colloid Interf Sci. 2011; 354: 429-436.
- Miao J, Su J, Wen Y, Rao W. Preparation, characterization and photoluminescence of Sm³⁺ doped NaGdF₄ nanoparticles. J Alloy Compd. 2015; 636: 8-11.
- 18. Lei L, Chen D, Huang P, Xu J, Zhang R, Wang Y. Modifying the size and uniformity of up conversion Yb/Er: NaGdF₄ nanocrystals through alkalineearth doping. Nanoscale. 2013; 5: 11298-11305.
- Xu J, Lv R, Du S, Gai S, He F, Yang D, et al. UCNPs@gelatin-ZnPc nanocomposite: synthesis, imaging and anticancer properties. J Mater Chem. B. 2016; 4: 4138-4146.
- 20. He M, Huang P, Zhang C, Hu H, Bao C, Gao G, et al. Dual Phase-Controlled Synthesis of Uniform Lanthanide-Doped NaGdF₄ Up conversion Nanocrystals Via an OA/Ionic Liquid Two-Phase System for In Vivo Dual-Modality Imaging. Adv Funct Mater. 2011; 21: 4470-4477.

 Liu C, Wang H, Zhang X, Chen D. Morphology- and phase-controlled synthesis of monodisperse lanthanide-doped NaGdF₄ nanocrystals with multicolor photoluminescence. J Mater Chem. 2009; 19: 489-496.

- 22. Zhang Y, Das GK, Vijayaragavan V, Xu QC. Padmanabhan, P; Bhakoo, KK; Selvan, ST; Tan, TTY "Smart" theranostic lanthanide nanoprobes with simultaneous up-conversion fluorescence and tunable T₁-T₂ magnetic resonance imaging contrast and near-infrared activated photodynamic therapy. Nanoscale. 2014; 6: 12609-12617.
- Shao C, Li S, Gu W, Gong N, Zhang J, Chen N, et al. Multifunctional Gadolinium-Doped Manganese Carbonate Nanoparticles for Targeted MR/ Fluorescence Imaging of Tiny Brain Gliomas. Anal Chem. 2015; 87: 6251-6257.
- 24. Zhai X, Lei P, Zhang P, Wang Z, Song S, Xu X, et al. Growth of lanthanide-doped LiGdF₄ nanoparticles induced by LiLuF₄ core as tri-modal imaging bioprobes. Biomaterials. 2015; 65: 115-123.
- Liu Q, Sun Y, Li C, Zhou J, Li C, Yang T, et al. 18 F-Labeled Magnetic-Up conversion Nanophosphorsvia Rare-Earth Cation-Assisted Ligand Assembly. ACS Nano. 2011; 5: 3146-3157.
- Yang C, Liu Q, He D, Na N, Zhao Y, Ouyang J. Dual-modal imaging and photodynamic therapy using up conversion nanoparticles for tumor cells. The Analyst. 2014; 139: 6414-6420.
- Huang J, Hou Y, Liu C, Jing L, Ma T, Sun X, et al. Chemical Spacer Design for Engineering the Relaxometric Properties of Core-Shell Structured Rare Earth Nanoparticles. Chem Mater. 2015; 27: 7918-7925.
- 28. Chen D, Huang P. Highly intense up conversion luminescence in Yb/Er: NaGdF₄@NaYF₄ core-shell nanocrystals with complete shell enclosure of the core. Dalton Trans. 2014; 43: 11299-11304.
- 29. Quintanilla M, Ren F, Ma D, Vetrone F. Light Management in Up converting Nanoparticles: Ultra small Core/Shell Architectures to Tune the Emission Color. ACS Photonics. 2014; 1: 662-669.
- 30. Chen G, Ohulchanskyy TY, Liu S, Law W, Wu F, Swihart MT, et al. Core/ Shell NaGdF₄:Nd³⁺/NaGdF₄ Nanocrystals with Efficient Near-Infrared to Near-Infrared Down conversion Photoluminescence for Bioimaging Applications. ACS Nano. 2012; 6: 2969-2977.
- 31. Yu S, Cao R, Li J, Meng L. Controlled synthesis of NdF₃ and NaNdF₄ microor nanocrystals by one-pot microwave-assisted hydrothermal reaction. J Fluorine Chem. 2015; 178: 286-290.
- Deng Y, Wang H, Gu W, Li S, Xiao N, Shao C, et al. Ho³⁺ doped NaGdF₄ nanoparticles as MRI/optical probes for brain glioma imaging. J Mater Chem B. 2014: 2: 1521-1529.
- 33. Zhao Q, Shao B, LüW, Lv W, Jiao M, Zhao L, et al. β -NaGdF $_4$ nanotubes: one-pot synthesis and luminescence properties. Dalton Trans. 2015; 44: 3745-3752.
- 34. Guan H, Liu G, Wang J, Dong X, Yu W. Tunable luminescence and energy transfer properties of NaGdF₄:Dy³⁺, Eu³⁺ nanophosphors. New J Chem. 2014; 38: 4901-4907.
- 35. Guan H, Liu G, Wang J, Dong X, Yu W. Multicolor tunable luminescence and paramagnetic properties of NaGdF₄:Tb³⁺/Sm³⁺ multifunctional nanomaterials. Dalton Trans. 2014; 43: 10801-10808.
- 36. Li X, Hanagata N, Wang X, Yamaguchi M, Yi W, Bando Y, et al. Multimodal luminescent-magnetic boron nitride nanotubes@NaGdF₄:Eu structures for cancer therapy. Chem Commun. 2014; 50: 4371-4374.
- 37. Huang X. Realizing efficient up conversion and down-shifting dual-mode luminescence in lanthanide-doped NaGdF4 core-shell-shell nanoparticles through gadolinium sublattice-mediated energy migration. Dyes and Pigments. 2016; 130: 99-105.
- Jiao M, Jing L, Liu C, Hou Y, Huang J, Wei X, et al. Differently sized magnetic/ up conversion luminescent NaGdF₄: Yb, Er nanocrystals: flow synthesis and solvent effects. Chem Commun. 2016; 52: 5872-5875.